Proceedings of the National Academy of Sciences of the United States of America
April 2013, Volume 110 (17), Pages 6682-6687
http://dx.doi.org/10.1073/pnas.1214676110

Abrupt drainage cycles of the Fennoscandian Ice Sheet

Guillaume Soulet[a, b, *], Guillemette Ménot[a], Germain Bayon[b], Frauke Rostek[a], Emmanuel Ponzevera[b], Samuel Toucanne[b], Gilles Lericolais[b], and Edouard Bard[a, *]

[a] Aix Marseille Université, Centre National de la Recherche Scientifique, Institut de Recherche pour le Développement, Collège de France and Centre Européen de Recherche et d'Enseignement des Géosciences de l'Environnement Unité Mixte 34, 13545 Aix-en-Provence Cedex 04, France
[b] Institut Français de Recherche pour l'Exploitation de la Mer, Centre de Brest, 29280 Plouzané Cedex, France.

*: Corresponding authors : Guillaume Soulet, email address : soulet@cerege.fr ; Edouard Bard, email address : bard@cerege.fr.

Abstract:

Continental ice sheets are a key component of the Earth's climate system, but their internal dynamics need to be further studied. Since the last deglaciation, the northern Eurasian Fennoscandian Ice Sheet (FIS) has been connected to the Black Sea (BS) watershed, making this basin a suitable location to investigate former ice-sheet dynamics. Here, from a core retrieved in the BS, we combine the use of neodymium isotopes, high-resolution elemental analysis, and biomarkers to trace changes in sediment provenance and river runoff. We reveal cyclic releases of meltwater originating from Lake Disna, a proglacial lake linked to the FIS during Heinrich Stadial 1. Regional interactions within the climate–lake–FIS system, linked to changes in the availability of subglacial water, led to abrupt drainage cycles of the FIS into the BS watershed. This phenomenon raised the BS water level by ~100 m until the sill of the Bosphorus Strait was reached, flooding the vast northwestern BS shelf and deeply affecting the hydrology and circulation of the BS and, probably, of the Marmara and Aegean Seas.

1. Main text

Despite the prominent role of large continental ice sheets in past climate changes (1), our understanding of ice dynamics is still insufficient to predict the retreat of modern ice sheets (2–4).

Reconstructing the deglacial demise of former ice sheets is thus of crucial interest to further understand the mechanisms underlying modern ice-sheet dynamics and can be done by studying sediment archives retrieved off large river systems that drained the decaying ice sheets during the last deglaciation (5–7).

The Eurasian Fennoscandian Ice Sheet (FIS) formed the second-largest ice mass of the Northern Hemisphere (8) (Fig.1A). Early deglacial history of the FIS southwestern flank has been improved through studies of sediment archives collected in the Bay of Biscay. Between 20 ka and 17 ka (all ages are reported in calendar age before the present), meltwater emanating from the decay of FIS southwestern margins was routed toward the North Atlantic through the “English Channel mega-river” (6, 7) (Fig. 1A). At around 17 ka, rapid motion of the ice tongue over the present North Sea diverted meltwater flow toward the Nordic Seas, bringing about the cessation of the English Channel mega- river activity (7).

By contrast, despite numerous field investigations (8, 9) and extensive morainic dating (10), little is known about meltwater routing for the FIS southeastern flank (11). The potential of Black Sea (BS) sediments as an archive of the deglacial history of this FIS sector (Fig. 1A) was recently suggested by the discovery of peculiar sedimentary structures known as the Red Layers (RLs). RLs are a series of four individualized intervals of red- dish-brown clays and are thought to represent the sedimentary imprints of the meltwater inputs (12–15) that occurred during Heinrich Stadial 1 (HS1) (16). To date, however, the genesis and origin of the RLs remain enigmatic, even if three main hypotheses have been proposed to account for their occurrence in BS sediment sequences.

The first, and traditional, hypothesis suggests that the RLs were deposited in response to the deglacial spillover of the Caspian Sea into the BS via the Manych Depression and the Sea of Azov (12, 17, 18). In this scenario, the Caspian spillover would have been mainly caused by high surface runoff within the Volga catchment area due to the combination of reduced vegetation cover, increased seasonality favoring snow accumulation during long winter and rapid spring melting, and widespread permafrost (19, 20). This would have resulted in enhanced Volga River run- off, raising the water level of the Caspian Sea and causing its outflow into the BS. The FIS contributed to only a minor extent in the Caspian transgression (19–21). The second hypothesis suggests that deposition of the RLs was directly linked to FIS recession north of the Dniepr drainage basin. Indeed, early in the last deglaciation, the retreat of the FIS led to the formation of proglacial Lake Disna, which developed within a basin where it was constrained to the north by the FIS and to the south by the northern limit of the BS drainage basin (22) (Fig. 1B).

During HS1, the possible drainage of proglacial Lake Disna through the headwaters of the Dniepr River could have supplied meltwater to the BS (23) (Fig. 1B) and led to the deposition of the RLs. Therefore, reconstructing the activity of the Dniepr River from sediments of the BS could provide a continuous record of FIS deglacial history. Alternatively, and as a third hypothesis, the HS1 recession of the Alpine Ice Cap (24, 25) could also have released volumes of meltwater to the BS via the Danube River (Fig. 1A), potentially making the RLs alpine in origin (further information Q: 12 is given in SI Text).

To constrain the geographical origin of the RLs and to ascertain their meltwater-induced deposition, we measured inorganic tracers for sediment provenance [X-ray fluorescence

(XRF) Ti/Ca ratio and eNd signatures] and biomarkers as proxies for terrigeneous supply to the BS [branched and isoprenoid tetraether (BIT) index and C25-alkane/total organic carbon (TOC)] in the well-dated core MD04-2790 (16, 26) collected in the near vicinity of the mouths of the Danube and the Dniepr Rivers (Fig.1A). By focusing on the temporal organization of the RLs, we highlight the dynamic interplay within the climate–FIS–Lake Disna system that led to the cyclic drainage of the lake into the BS.

Before 15 ka, XRF-Ti/Ca records from BS sediments represent a qualitative tracer for changes in sediment provenance (13). The eNd signature of terrigenous sediments is a powerful and sensitive tracer for sediment provenance because it is retained during continental weathering and subsequent transport (27, 28). The BS drainage basin displays highly contrasted eNd signatures (indicative values in Fig. 1A; a more detailed map is shown in Fig. S1). Thus, large changes in eNd are expected in our sedi- mentary archive, making for easier identification of the geo- graphical source of RLs. The BIT index is a proxy for terrestrial vs. aquatic organic matter supply to sediments and can be useful in investigating changes in the delivery of soil organic matter fluvially transported to an aquatic system (6, 29). In combination with the BIT index, we measured the C25-alkane/TOC profile. Odd midchain C25-alkane was found to be a biomarker for Sphagnum moss species, a dominant vegetation component in wetlands and peats (30, 31). C25-alkane/TOC measured in the sediment is there therefore expected to reflect terrestrial organic matter transported by rivers and surface runoff and thus provide additional information to trace terrestrial organic deliveries into the BS.

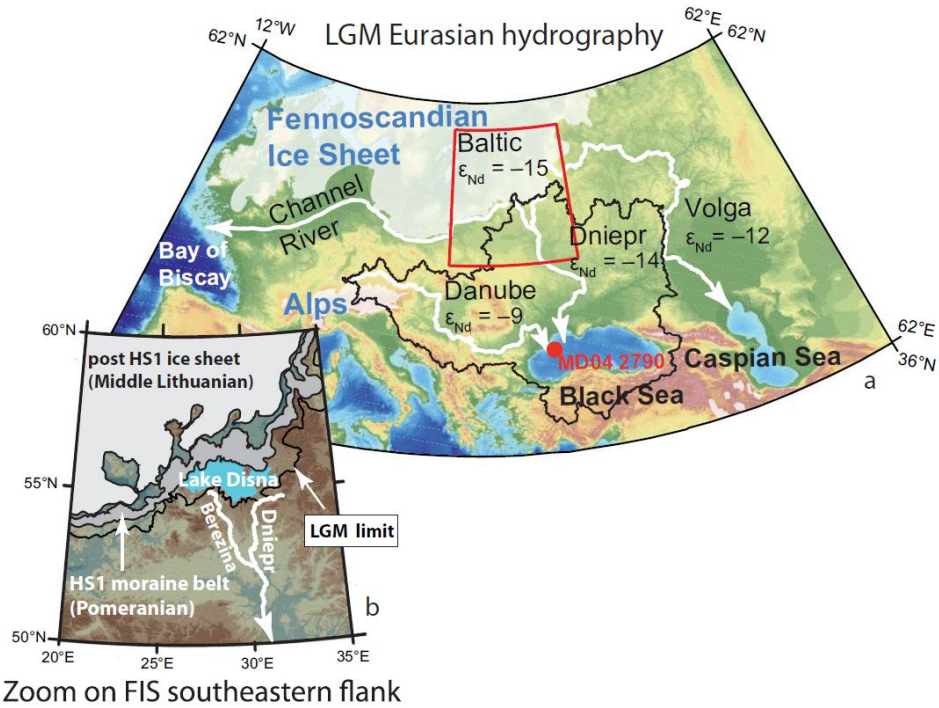

Fig. 1. **(A)** The LGM hydrographic network of the Eurasian continent. Baltic rivers were diverted westward by the FIS, creating the “English Channel mega-river,” which flowed into the Bay of Biscay. In northeastern Europe, the FIS reached the northern limit of the BS drainage basin; hence, no substantial meltwater release seems to have reached the BS before FIS early deglacial retreat. During the Last Deglaciation, the Alpine Ice Cap potentially delivered meltwater to the BS via the Danube River. To trace meltwater contribution to the BS, representative eNd signatures of the Dniepr and Danube basins, as well as of the Baltic region, are indicated (Fig. S1 shows a more detailed map). The main rivers draining

European ice masses are represented in thick white. The BS drainage basin is represented by a thick black line. Basin water levels are lowered by 120 m to account for LGM water levels. Core MD04-2790 (red circle) was taken during an ASSEMBLAGE cruise aboard RV Marion Dufresne.
(B) Compiled ice-margin positions of the FIS southeast of the Baltic Sea (9, 22). The LGM moraine, the HS1 moraine belt (Pomeranian), and the post-HS1 ice sheet (Middle Lithuanian) are shown. Lake Disna is represented in blue.

2. Results and Discussion

As shown in Fig. 2, the BIT index and C25-alkane/TOC ratio display very similar patterns, implying that both markers success- fully trace terrestrial organic matter inputs to the BS. Before 15 ka, both proxies show a baseline suddenly disrupted by four prominent peaks during HS1 (orange bars in Fig. 2 A and B). Subsequently, both proxies show a baseline suddenly disrupted by four prominent peaks during HS1 (orange bars in Fig. 2 A and B). Subsequently, both proxies show a decreasing trend throughout the Late Glacial (between 15–10 ka) with lower values than during the Glacial (before 15 ka) (Fig. 2A). This pattern suggests that terrestrial input to the BS was lower during the Late Glacial than during the Glacial, probably as a result of higher glacial surface runoff owing to reduced vegetation cover and widespread permafrost (20, 32). The proxy values peak within the RLs and return to glacial background values in between (orange bars in Fig. 2 A and B), suggesting that throughout HS1 terrestrial input was similar to that of the Glacial, except for four episodes of substantial additional delivery of terrestrial organic matter to the BS. Because each RL is associated with a 1‰ negative excursion in water δ18O (12, 13, 15), these phases of increase in river runoff, called here BS water pulses (BSWPs), are associated with large releases of meltwater related to the decay of the surrounding ice masses.

Our εNd record reveals the geographical origin of the BSWPs. Whereas throughout the record εNd signatures remain remarkably constant (average −11.3 ± 0.3, n = 53), each RL is characterized by a prominent drop in εNd values (Fig. 2 A and B). Such negative εNd values reveal the presence of one very unradiogenic component within the sediments. Among the possible geographical sources proposed for the BSWPs, only the Baltic and Dniepr (including the lower course crossing the Ukrainian Shield) terrains are characterized by such a signature (Fig. 1A and SI Text). In this region, the only meltwater reservoir that could have been connected to the BS watershed was proglacial Lake Disna, and it drained via the headwaters of the Dniepr River (23) (Fig. 1B).

Interestingly, in the Baltic and Upper Dniepr areas, reddish tills deposited during the Last Glacial epoch are regionally widespread (33) and overall are present along the course of the Berezina River (22). The Berezina River is a large tributary of the Upper Dniepr River and was directly connected to Lake Disna, lending strength to the suggestion that the clay fraction of RLs originates from drainages of Lake Disna (Fig. 1B). Both the geochemical signatures of our records and the regional occur- rence of reddish till thus suggest that sudden drainages of Lake Disna delivered large volumes of meltwater that were responsible for the BSWPs ~1,200 km away (Fig. 1A). The meltwater floods would thus have led to the erosion of the uppermost glacial sedimentary deposits and subsequent transport into the BS of the reddish clays via the Berezina and Dniepr Rivers. RLs therefore represent the southernmost sedimentary imprint of the deglacial history of the southeastern flank of the FIS.

A close up of the RLs (Fig. 2B) provides insights into the dynamic interplay between climate, FIS, and proglacial Lake Disna. First, abrupt transitions in the XRF-Ti/Ca signature of each

RL (Fig. 2 A and B) imply instantaneous onset and cessation of each associated BSWP. As revealed by microscopic investigations of thin sediment sections, each BSWP is composed characteristically of ~220 successive seasonal floods, as shown by our detailed study of the chronology of core MD04-2790 (16). This feature implies that each BSWP represents repeated sea- sonal drainages of Lake Disna over ~220-y-long periods. BSWP periods are then followed by ~200-y-long periods of regular runoff (Fig. 2B). This pattern, together with the lack of random distribution of BSWPs in the sedimentary sequence, calls for dynamic interactions within the FIS–lake system causing cyclic drainages of Lake Disna during HS1.

Field investigations (Fig. 1B) provide additional key clues to understanding the sequence of events that led to the cyclic drainages of the lake. Lake Disna was constrained by the Last Glacial Maximum (LGM) moraine to the south and dammed by the HS1 margin of the FIS to the north (Fig. 1B). It has been suggested that Lake Disna led to a faster regional decay of the FIS through passive glacier thinning and calving (22). This passive regime of ice retreat was followed by a prolonged phase of ice-front stagnation leading to the formation of the HS1 moraine belt (22) (Fig. 1B). Ice stagnation was interrupted by a series of short pulses of ice advance, as is suggested by the formation of pushed moraine ridges within the HS1 moraine belt (22). Concomitant with the BSWPs, the pulses of ice advance may have triggered cyclic spillovers of Lake Disna toward the BS.

We propose that cyclic drainages of Lake Disna were triggered by changes in the basal buoyancy of the ice-sheet margin, which itself relied upon the availability of subglacial water (Fig. 3 shows a schematic view of the proposed mechanisms). Indeed, changes in the basal effective pressure (ice overburden minus subglacial water pressures) lead either to enhanced basal buoyancy and sub- sequent ice-sheet gravitational collapse when subglacial pressure stabilization (34–37).

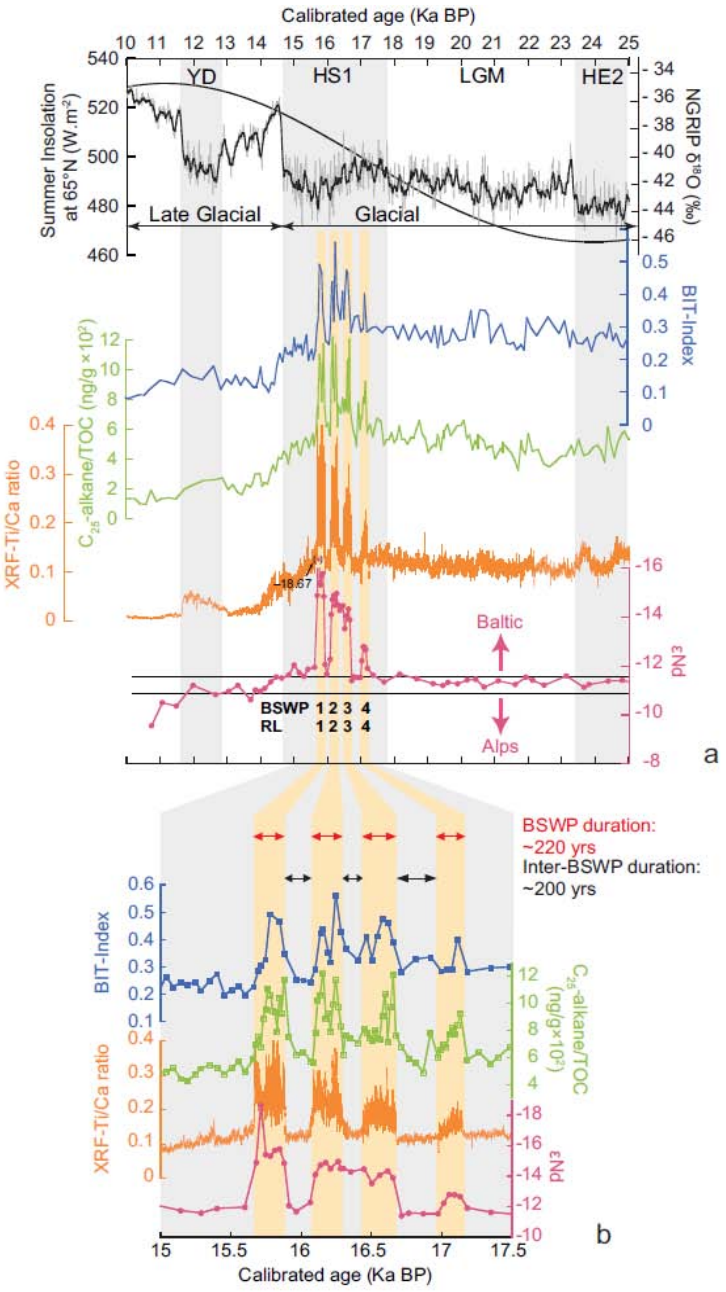

Fig. 2. Deglaciation records of the activity of rivers flowing into the BS and of the provenance of the transported sediments, compared with global paleoclimatic changes. Climatic cold spells are labeled as follows: HE2, Heinrich Event 2; HS1, Heinrich Stadial 1, as defined by ref. 48, which is equivalent to the Mystery Interval of ref. 49; YD, Younger Dryas. (A) The upper panel shows δ18O in NGRIP ice core (50) and summer insolation at 65°N (51). Curves below the upper panel refer to records obtained from core MD04-2790. The blue curve is the BIT index (data previously presented in ref. 52 only to correct TEX86 paleotemperatures). The green curve is the C25-alkane/TOC. The orange curve is XRF-Ti/Ca (16). The pink curve is the eNd record of the clayey fraction. The four RLs and corresponding BSWPs are labeled from 1 to 4 and are represented by orange bands. (B) Detail of the RLs between 15–17.5 ky B.P. The same records are presented. Red and black arrows show the duration of each BSWP as well as the duration of periods of regular runoff (inter-BSWP). The chronology of core MD04-2790 is based on 28 radiocarbon ages and was refined by varve counting and tuning to climatic series of reference (16, 26).

An early retreat of the FIS from its LGM maximal extent occurred due to increasing Northern Hemisphere summer in- solation and led to the creation of proglacial Lake Disna ("ice margin retreat" in the "filling loop" of Fig. 3). Lake Disna initially increased in size over ca. 3,000 y between ~20 ka (10) and ~17 ka, at which time the first BSWP occurred (16). Lake level rise caused the formation of a calving wall at the ice front. After the lake level was sufficiently high, the calving front was set afloat, turning it into a short ice shelf and resulting in the retreat of the grounding line (35). Then, lake water spread into the glacier, causing an increase in basal buoyancy and lubrication upstream of the grounding line (Fig. 3). This triggered ice-mar- gin thinning and acceleration (Fig. 3) and the attendant in- creased calving rate (34–37) (Fig. 3). The initial filling of Lake Disna was then suddenly disrupted during HS1, suggesting that this climatic cold spell played a key role in the FIS–lake system by triggering centennial cyclic drainages of Lake Disna.

The shortening of the HS1 melting season (38) altered the balance between the rates of ice input and melting of ice in Lake Disna. When ice input through calving exceeds loss through melting, the FIS–lake system switched from the filling loop to the drainage loop (Fig. 3). Lake Disna filled with icebergs, leading to ice-margin buttressing (39, 40). Consequently, the ice margin advanced (Fig. 3). The partial refilling with ice of the proglacial depression caused the spillover of unfrozen water, leading to drainage of Lake Disna and the attendant BSWP (Fig. 3). Additionally, the ice-margin advance flushed out pressurized sub- glacial water from the glacier base, a phenomenon that occurs in modern settings (36) and that can be inferred from modeling (41). Through the reduction of subglacial water availability, both phenomena diminish subglacial buoyancy, leading to increased basal friction. In consequence, ice-margin advance ultimately decelerated (Fig. 3), further reducing FIS input of ice through calving to Lake Disna (Fig. 3). After the rate of ice melting exceeded the rate of ice input to the lake (Fig. 3), lake drainage ceased and the FIS–lake system switched to the filling loop (Fig. 3). We hypothesize that this mechanism ended when the FIS retreated far enough north to drain Lake Disna toward the Baltic basin (Fig. 1B). Indeed, the early stage of Baltic Sea filling occurred at ca. 16–15 ka (11, 23), which lends support to the concomitant disappearance of water pulses observed in the BS (15.7 ± 0.3 ka) (16).

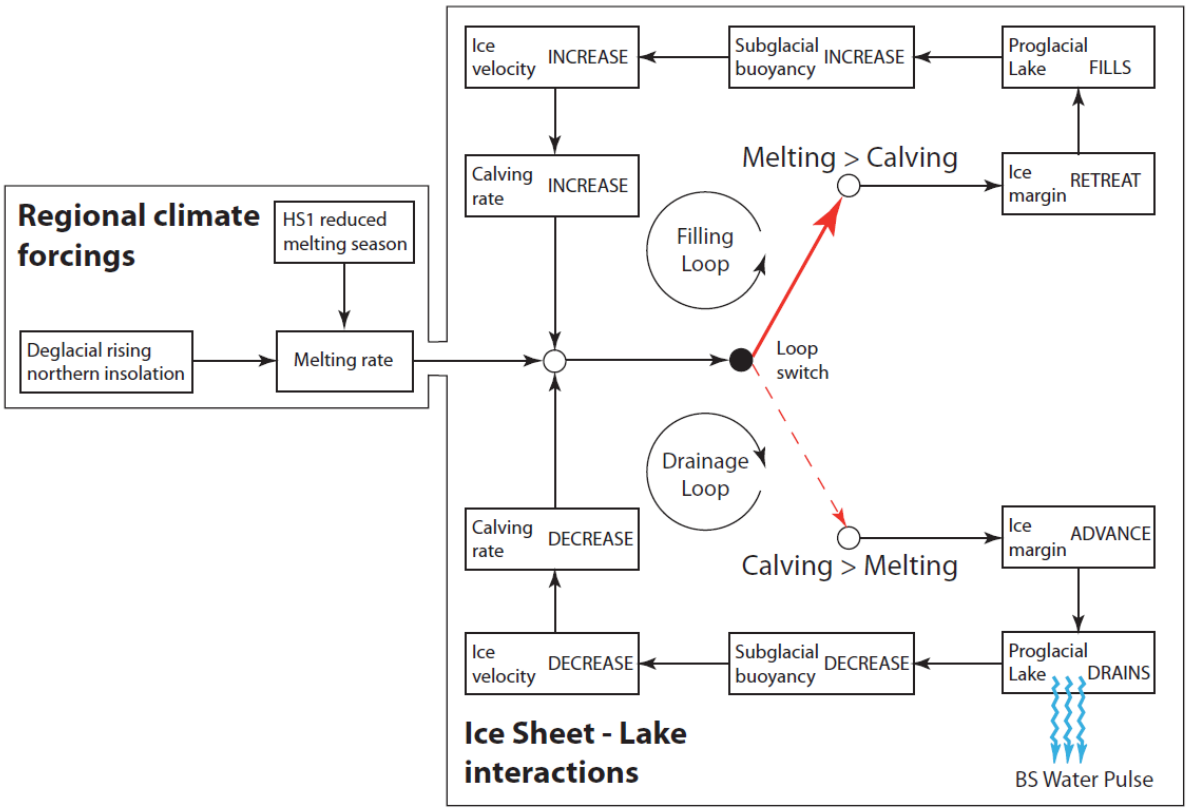

Fig. 3. Schematic representation of the HS1 cyclic drainages of Lake Disna. Filling loop: the retreating ice margin causes growth of the proglacial lake, leading to increased subglacial buoyancy. This thereby increases ice velocity and the associated calving rate. When calving exceeds iceberg melting within Lake Disna, the FIS–lake system switches to the drainage loop: The ice margin advances, flushing lake water into the BS drainage basin (BSWP). This decreases subglacial buoyancy, thus diminishing both ice velocity and the calving rate. The drainage phase persists until the rate of iceberg melting exceeds the rate of iceberg input (calving rate).

The repeated large volumes of meltwater released from Lake Disna to the Dniepr catchment would have led to the progressive development of a pathway between the two basins. Interestingly, each RL is characterized by geochemical signatures that are higher in amplitude than the preceding ones (Fig. 2). Sedimentation rates also increase from one RL to the next (sedimentation rates from the oldest RL (RL4) to the youngest (RL1) are 260, 265, 280, and 305 cm/ky, respectively (16)). These observations very likely lend support to the idea that the pathway connecting Lake Disna to the Dniepr basin may have been progressively enlarged by the successive phases of erosion triggered by the four centennial periods of BSWPs. This connection would have been directly dependent on the water level in Lake Disna (centennial cycles linked to the above-described FIS–lake dynamic system) and, during the BSWPs, upon the physical state of the water (ice or liquid according to seasonal cycle, i.e., autumn–winter vs. spring–summer).

Our results reveal that ice-sheet dynamics can be extremely unstable depending on subtle changes within the climate–ice sheet–lake system. They could provide new clues to further understand the regional ice-sheet surges that characterized the late glacial history of both the Laurentide and Fennoscandian Ice Sheets (42, 43). Additionally, to the south, the hydrology of the BS was also strongly affected by the cyclic drainage of Lake Disna. The increase in runoff due to repeated seasonal floods over four successive periods of ~220 y raised the BS water level by around 100 m, until the sill of the Bosphorus Strait was reached (12, 13, 16, 44, 45), leading to the flooding of the vast northwestern shelf of the BS basin and the attendant drastic retreat of the coastline (SI Text). The resulting outflow of BS waters into the northeastern Mediterranean basins altered the hydrology of both the Marmara Sea (45) and the Aegean Sea (46, 47). In the Aegean Sea, a drop in deep-water oxygenation is recorded during HS1 (46, 47), suggesting that the reduction in the formation of North Aegean deep water could have been caused by the injection of fresh water from the BS. Further investigation in the Eastern Mediterranean Sea is needed to evaluate the complex interactions between the BS outflow and the Mediterranean thermohaline circulation. Finally, our results provide complementary information related to Eurasian meltwater routing and proglacial lake effects on climate and environment from regional to continental scales, and to the understanding of the Last Deglaciation on the global scale.

3. Materials and Methods

3.1. Studied Core

Piston core MD04-2790 was recovered in the upper slope of the northwestern BS (44°12.8′N, 30°59.6′E; 352-m water depth) in the axis of both the Danube and Dniepr rivers during the 2004 Assessment of the Black Sea Sedimentary System Since the Last Glacial Extreme (ASSEMBLAGE)-1 cruise, aboard the RV Marion Dufresne. The coring site was chosen on the basis of a seismic profile that had been determined during the Ifremer BlaSON2 survey in 2002 and was shot on the slope outside the Danube Canyon system. The seismic profile

shows a thick sediment sequence that presents a regular succession of layers that are neither deformed nor structured by tectonic movements (53). Both the seismic profile and the careful inspection of the core sediments reveal continuous hemipelagic sedimentation. From the top of the core to a depth of 1.24 m, the sample revealed the typical marine stratigraphic units I and II (54). The lowermost limnic unit, unit III (54), was found from a depth of 1.24 m to the core base (16). The geochemical substratigraphy of unit III is extensively described in ref. 16 and is in full agreement with other cores recovered in the western BS (12–15, 17, 44, 55, 56). Core MD04-2790 chronology is based on 28 radiocarbon ages and was refined by varve counting and tuning to climatic series of reference (16, 26). The varve chronology concerns exclusively the RL interval. The varved pattern was initially suggested by the visual investigation of the core sediment and further studied by X-ray imagery and microphotography of sediment thin sections. Each RL (RL1 to RL4 in Fig. 2) consists of a succession of greenish and red laminations corresponding to X-ray bright and dark laminations, respectively (see figure 4 in ref. 16). The microphotographs of the sediment thin sections reveal that each red lamination is characterized by a high amount of scattered silt and sands embedded in a reddish clayey matrix, suggesting that the silt and sands represent ice rafted debris. Comparatively, each greenish lamination is characterized by rare silts and sands embedded in a “regular” greenish clayey matrix (see figure 4 in ref. 16). These features are interpreted as representing the expulsion of the so-called ice anchor (i.e., ice attached to the bed of rivers and including bed materials) by meltwater discharges of northwest BS rivers during the melting season (red laminations), alternating with regular river runoff during the rest of the year (greenish laminations). Radiocarbon age controls support seasonal deposition of the red laminations (16). This core continuously covers the last 40 ka, including the Last Deglaciation, on which this study is focused. Sedimentation rates are high, ranging from 0.2 to 0.4 m/ky during the Late Glacial (15–10 ka) to more than 3 m/ky during the Red Layer interval (RLs), the period corresponding to the water pulses. During the Glacial, the sedimentation rate reached 1 m/ky (16). We sampled 1-cm-thick slices of sediments for geochemical analysis (discussed below).

3.2. Total Organic Carbon, C25-Alkane Concentrations, and BIT Index

TOC was measured at the Centre Européen de Recherche et d’Enseignement des Géosciences de l’Environnement (CEREGE) with a gas chromatographic elemental analyzer as described in ref. 57. Data were presented in ref. 16. For lipid analysis, performed at CEREGE, 1–5 g of sediment was extracted for biomarkers using the accelerated solvent extraction method (ASE 200 system; Dionex) at 120 °C and 100 bars with dichloromethane/methanol (9:1 vol/vol). Aliquots were split and a third of each was directly injected into a gas chromatograph (GC) for n-alkane analysis. GC analyses (Table S1) were performed using a flame ionization detector-equipped Fisons Instruments GC8065 and Thermo Electron Trace GC, a 60-m × 0.25-mm × 0.1-μm nonpolar fused silica column DB-5-MS (J&W) fitted with a 2.5-m × 0.53-μm deactivated retention gap and hydrogen as a carrier gas. Molecular identification was checked by GC-MS (DSQ; Thermo) on selected samples. For analyses of glycerol dialkyl glycerol tetraethers (GDGTs) (Table S2), as described in ref. 52, the total lipid extract was subsequently separated into polar and apolar fractions by means of a column packed with Al2O3 using hexane/dichloromethane (9:1, vol/vol) and dichloromethane/methanol (1:1, vol/vol) as eluents, respectively. The polar fraction was then filtered through a 0.45-μm, 4-mm-diameter pPolytetrafluoroethylene filter before injection. GDGTs were quantified at the CEREGE by HPLCy/atmospheric pressure chemical ionization mass spectrometry using positive ions on an HP-LC-MS1100 Series. Analytical conditions were similar to those described in ref. 29. BIT-index values were calculated according to ref. 29. Mean analytical precision on the BITindex values is 0.008. Results from our laboratory were found to compare favorably with data from other laboratories (58).

3.3. Neodymium Isotopes Measurements

After sieving for the clays, each carbonate- free sediment sample was dissolved by alkaline fusion following the method recommended by ref. 59. Organic matter was removed by leaching them with a solution of 4% H2O2. Neodymium was separated from other light rare earth elements by miniaturized extraction chromatography (60). Ratios of $^{143}Nd/^{144}Nd$ were measured by multicollector–inductively coupled plasma–MS at L'Institut Français de Recherche pour l'Exploitation de la Mer (Brest, France) with a Thermo Neptune. All $^{143}Nd/^{144}Nd$ ratios were corrected for mass discrimination using $^{146}Nd/^{144}Nd = 0.7219$ with an exponential law model (61). La Jolla Nd isotopic standard ($^{143}Nd/^{144}Nd = 0.511858$) measurements were performed to bracket two unknown samples for result normalization. Measurements of JNdi-1 isotopic standard and BHVO-2 (US Geological Survey basalt reference material) were performed in every analytical session to assess accuracy and external repeatability. JNdi-1 solutions were prepared from a stock bottle, whereas BHVO-2 underwent the same chemical treatment as all samples for each measurement session. Results obtained for these materials are $^{143}Nd/^{144}Nd = 0.512113 \pm 2$ ($2_{\zeta m}$, n = 64) and $^{143}Nd/^{144}Nd = 0.512991 \pm 4$ ($2_{\zeta m}$, n = 16) for JNdi-1 and BHVO-2, respectively. These results are in agreement with previously published data (62, 63). Measured $^{143}Nd/^{144}Nd$ ratios are reported in ε notation (in parts per 104) (Table S3). εNd represents the relative deviation of the sample $^{143}Nd/^{144}Nd$ ratio, from that of the CHUR reference (CHondritic Uniform Reservoir):

$[(^{143}Nd/^{144}Nd)_{sample}/(^{143}Nd/^{144}Nd)_{CHUR} - 1] \times 10^4$. Here, εNd is calculated relative to $(^{143}Nd/^{144}Nd)_{CHUR}$ 0.512638 (64). Uncertainties for εNd are reported as 2ζ. The mean uncertainty is 0.13 ε unit for a single analysis.

Acknowledgments

We thank J. Etoubleau at L'Institut Français de Recherche pour l'Exploitation de la Mer (Ifremer) for technical assistance during X-ray fluorescence data acquisition and for help in the laboratory and B. Hoogendoorn, A. Matoshko, G. Vaikutiene, V. Zelchs, and H. Vallius for the collection of modern sediment samples of rivers. G.S. thanks Centre National de la Recherche Scientifique, Ifremer, and the Collège de France for providing salary support. Paleoclimate work at Centre Européen de Recherche et d'Enseignement des Géosciences de l'Environnement is supported by grants from the Gary Comer Foundation for Science and Education, the European Community (Project Past4Future), and the Collège de France (to E.B.). Core MD04-2090 was collected by the RV Marion Dufresne supported by the Institut Polaire Français. This work is a contribution to the Assessment of the Black Sea Sedimentary System Since the Last Glacial Extreme project conducted by G.L. and funded by European Commission Grant EVK3-CT-2002-00090.

References

1. Clark PU, Alley RB, Pollard D (1999) Northern Hemisphere ice-sheet influences on global climate change. Science 286(5442):1104–1111.

2. Jacob T, Wahr J, Pfeffer WT, Swenson S (2012) Recent contributions of glaciers and ice caps to sea level rise. Nature 482(7386):514–518.

3. Meehl GA, et al. (2007) Global Climate Projections. Climate Change 2007: The Physical Science Basis. Contribution of Working Group I to the Fourth Assessment, Report of the Intergovernmental Panel on Climate Change, eds Solomon S, et al. (Cambridge Univ Press, Cambridge, UK), pp 747–845.

4. Pfeffer WT, Harper JT, O'Neel S (2008) Kinematic constraints on glacier contributions to 21st-century sea-level rise. Science 321(5894):1340–1343.

5. Flower BP, Hastings DW, Hill HW, Quinn TM (2004) Phasing of deglacial warming and Laurentide Ice Sheet meltwater in the Gulf of Mexico. Geology 32(7):597–600.

6. Ménot G, et al. (2006) Early reactivation of European rivers during the last deglaciation.Science 313(5793):1623–1625.

7. Toucanne S, et al. (2010) The first estimation of Fleuve Manche palaeoriver dischargeduring the last deglaciation: Evidence for Fennoscandian ice sheet meltwater flow inthe English Channel ca 20-18 ka ago. Earth Planet Sci Lett 290(3–4):459–473.

8. Svendsen JI, et al. (2004) Late Quaternary ice sheet history of northern Eurasia. Quat. Sci Rev 23(11–13):1229–1271.

9. Ehlers J, Gibbard PL, Hughes PD (2011) Quaternary Glaciations: Extent and Chronology (Elsevier, Amsterdam), p 1108.

10. Rinterknecht VR, et al. (2006) The last deglaciation of the southeastern sector of the Scandinavian ice sheet. Science 311(5766):1449–1452.

11. Mangerud J, et al. (2004) Ice-dammed lakes and rerouting of the drainage of northern Eurasia during the Last Glaciation. Quat Sci Rev 23(11–13):1313–1332.

12. Bahr A, Arz HW, Lamy F, Wefer G (2006) Late glacial to Holocene paleoenvironmental evolution of the Black Sea, reconstructed with stable oxygen isotope records obtained on ostracod shells. Earth Planet Sci Lett 241(3–4):863–875.

13. Kwiecien O, et al. (2009) North Atlantic control on precipitation pattern in the eastern Mediterranean/Black Sea region during the last glacial. Quat Res 71(3):375–384.

14. Major C, Ryan W, Lericolais G, Hajdas I (2002) Constraints on Black Sea outflow to the Sea of Marmara during the last glacial-interglacial transition. Mar Geol 190(1–2):19–34.

15. Major CO, et al. (2006) The co-evolution of Black Sea level and composition through the last deglaciation and its paleoclimatic significance. Quat Sci Rev 25(17–18): 2031–2047.

16. Soulet G, et al. (2011) Black Sea "Lake" reservoir age evolution since the Last Glacial: Hydrologic and climatic implications. Earth Planet Sci Lett 308(1–2):245–258.

17. Bahr A, Lamy F, Arz H, Kuhlmann H, Wefer G (2005) Late glacial to Holocene climate and sedimentation history in the NW Black Sea. Mar Geol 214(4):309–322.

18. Ryan WBF, Major CO, Lericolais G, Goldstein SL (2003) Catastrophic flooding of the Black Sea. Annu Rev Earth Planet Sci 31(1):525–554.

19. Chepalyga AL (2007) The Black Sea Flood Question, eds Yanko-Hombach VV, Gilbert AS, Panin N (Springer, Heidelberg), pp 119–148.

20. Sidorchuk AY, Panin AV, Borisova OK (2009) Morphology of river channels and surface runoff in the Volga River basin (East European Plain) during the Late Glacial period. Geomorphology 113(3–4):137–157.

21. Lyså A, Jensen MA, Larsen E, Fredin OLA, Demidov IN (2011) Ice-distal landscape and sediment signatures evidencing damming and drainage of large pro-glacial lakes, northwest Russia. Boreas 40(3):481–497.

22. Karabanov AK, Matveyev AV (2011) Developments in Quaternary Sciences, eds Ehlers J, Gibbard PL, Hughes PD (Elsevier, Amsterdam), Vol 15, pp 29–35.

23. Kvasov DD (1979) The Late-Quaternary history of large lakes and inland seas of eastern Europe. Annales Academiae Scientiarum Fennicae AIII 127:1–71.

24. Schaefer JM, et al. (2006) Near-synchronous interhemispheric termination of the last glacial maximum in mid-latitudes. Science 312(5779):1510–1513.

25. Darnault R, et al. (2012) Timing of the last deglaciation revealed by receding glaciers at the Alpine-scale: Impact on mountain geomorphology. Quat Sci Rev 31:127–142.

26. Soulet G, Ménot G, Lericolais G, Bard E (2011) A revised calendar age for the last reconnection of the Black Sea to the global ocean. Quat Sci Rev 30(9–10):1019–1026.

27. Goldstein SJ, Jacobsen SB (1987) The Nd and Sr isotopic systematics of river-water dissolved material: Implications for the sources of Nd and Sr in seawater. Chem Geol 66(3-4):245–272.

28. Miller RG, O'Nions RK (1984) The provenance and crustal residence ages of British sediments in relation to palaeogeographic reconstructions. Earth Planet Sci Lett 68(3): 459–470.

29. Hopmans EC, et al. (2004) A novel proxy for terrestrial organic matter in sediments based on branched and isoprenoid tetraether lipids. Earth Planet Sci Lett 224(1–2): 107–116.

30. Eglinton G, Hamilton RJ, Raphael RA, Gonzalez AG (1962) Hydrocarbon constituents of the wax coatings of plant leaves: A taxonomic survey. Nature 193(4817):739–742.

31. Vonk JE, Gustafsson Ö (2009) Calibrating n-alkane Sphagnum proxies in sub-Arctic Scandinavia. Org Geochem 40(10):1085–1090.

32. Sidorchuk AY, Panin AV, Borisova OK (2011) Surface runoff to the Black Sea from the East European Plain during Last Glacial Maximum–Late Glacial time. Spec Pap Geol Soc Am 473:1–25.

33. Kalm V (2006) Pleistocene chronostratigraphy in Estonia, southeastern sector of the Scandinavian glaciation. Quat Sci Rev 25(9–10):960–975.

34. Bartholomew I, et al. (2010) Seasonal evolution of subglacial drainage and acceleration in a Greenland outlet glacier. Nat Geosci 3(6):408–411.

35. Hughes T (2003) Geometrical force balance in glaciology. J Geophys Res 108(B11): 2526.

36. Sole AJ, et al. (2011) Seasonal speedup of a Greenland marine-terminating outlet glacier forced by surface melt-induced changes in subglacial hydrology. J Geophys Res 116(F3):F03014.

37. Zwally HJ, et al. (2002) Surface melt-induced acceleration of Greenland ice-sheet flow. Science 297(5579):218–222.

38. Denton GH, Alley RB, Comer GC, Broecker WS (2005) The role of seasonality in abrupt climate change. Quat Sci Rev 24(10–11):1159–1182.

39. Amundson JM, et al. (2010) Ice mélange dynamics and implications for terminus stability, Jakobshavn Isbræ, Greenland. J Geophys Res 115(F1):F01005.

40. Geirsdóttir Á, Miller GH, Wattrus NJ, Björnsson H, Thors K (2008) Stabilization of glaciers terminating in closed water bodies: Evidence and broader implications. Geophys Res Lett 35(17).

41. Piotrowski JA (1997) Subglacial hydrology in north-western germany during the last glaciation: groundwater flow, tunnel valleys and hydrological cycles. Quat Sci Rev 16(2):169–185.

42. Bitinas A (2012) New insights into the last deglaciation of the south-eastern flank of the Scandinavian Ice Sheet. Quat Sci Rev 44:69–80.

43. Lowell TV, Larson GJ, Hughes JD, Denton GH (1999) Age verification of the Lake Gribben forest bed and the Younger Dryas Advance of the Laurentide Ice Sheet. Can J Earth Sci 36(3):383–393.

44. Bahr A, et al. (2008) Abrupt changes of temperature and water chemistry in the late Pleistocene and early Holocene Black Sea. Geochem Geophys Geosyst, 9(1), 10.1029/ 2007GC001683.

45. Vidal L, et al. (2010) Hydrology in the Sea of Marmara during the last 23 ka: Implications for timing of Black Sea connections and sapropel deposition. Paleoceanography 25(1):PA1205.

46. Kuhnt T, Schmiedl G, Ehrmann W, Hamann Y, Hemleben C (2007) Deep-sea ecosystem variability of the Aegean Sea during the past 22 kyr as revealed by Benthic Foraminifera. Mar Micropaleontol 64(3–4):141–162.

47. Schmiedl G, et al. (2010) Climatic forcing of eastern Mediterranean deep-water formation and benthic ecosystems during the past 22 000 years. Quat Sci Rev 29(23–24): 3006–3020.

48. Barker S, et al. (2009) Interhemispheric Atlantic seesaw response during the last deglaciation. Nature 457(7233):1097–1102.

49. Denton GH, Broecker WS, Alley RB (2006) The mystery interval 17.5 to 14.5 kyrs ago. PAGES News 14:14–16.

50. Andersen KK, et al.; North Greenland Ice Core Project members (2004) High-resolution record of Northern Hemisphere climate extending into the last interglacial period. Nature 431(7005):147–151.

51. Laskar J, et al. (2004) A long-term numerical solution for the insolation quantities of the Earth. Astron Astrophys 428(1):261–285.

52. Ménot G, Bard E (2012) A precise search for drastic temperature shifts of the past 40,000 years in southeastern Europe. Paleoceanography 27(2):PA2210.

53. Soulet G, et al. (2010) Glacial hydrologic conditions in the Black Sea reconstructed using geochemical pore water profiles. Earth Planet Sci Lett 296(1-2):57–66.

54. Ross DA, Degens ET (1974) The Black Sea: Geology, Chemistry, and Biology, eds Degens ET, Ross DA (Am Assoc Petroleum Geologists, Tulsa, OK), pp 183–199.

55. Kwiecien O, et al. (2008) Estimated reservoir ages of the Black Sea since the last glacial. Radiocarbon 50:99–118.

56. Ryan WBF (2007) The Black Sea Flood Question, eds Yanko-Hombach V, Gilbert AS, Panin N (Springer, Heidelberg), pp 63–88.

57. Pailler D, Bard E (2002) High frequency palaeoceanographic changes during the past 140,000 yr recorded by the organic matter in sediments of the Iberian Margin. Palaeogeogr Palaeoclimatol Palaeoecol 181(4):431–452.

58. Schouten S, et al. (2009) An interlaboratory study of TEX86 and BIT analysis using high-performance liquid chromatography mass spectrometry. Geochem Geophys Geosyst 10(3):Q03012.

59. Bayon G, et al. (2009) Determination of rare earth elements, Sc, Y, Zr, Ba, Hf and Th in geological samples by ICP-MS after Tm addition and alkaline fusion. Geostandards and Geoanalytical Research 33(1):51–62.

60. Pin C, Zalduegui JS (1997) Sequential separation of light rare-earth elements, thorium and uranium by miniaturized extraction chromatography: Application to isotopic analyses of silicate rocks. Anal Chim Acta 339(1–2):79–89.

61. Russell WA, Papanastassiou DA, Tombrello TA (1978) Ca isotope fractionation on the Earth and other solar system materials. Geochim Cosmochim Acta 42(8):1075–1090.

62. Tanaka T, et al. (2000) JNdi-1: A neodymium isotopic reference in consistency with LaJolla neodymium. Chem Geol 168(3–4):279–281.

63. Weis D, et al. (2006) High-precision isotopic characterization of USGS reference materials by TIMS and MC-ICP-MS. Geochem Geophys Geosyst 7(8):Q08006.

64. Jacobsen SB, Wasserburg GJ (1980) Sm-Nd isotopic evolution of chondrites. Earth Planet Sci Lett 50(1):139–155.